Supporting Information

Intercalated vs non-intercalated morphologies in donor-acceptor bulk heterojunction solar cells: PBTTT:fullerene charge generation and recombination revisited

Elisa Collado-Fregoso[1], *Samantha N. Hood*[2], *Safa Shoaee*[1], *Bob Schroeder*[3], *Iain McCulloch*[4,5], *Ivan Kassal*[2,6], *Dieter Neher*[1*] *and James R. Durrant*[4,7*]

[1]Department of Physics and Astronomy, University of Potsdam, Karl-Liebknecht-Straße 24–25,14476 Potsdam-Golm, Germany

[2]Centre for Engineered Quantum Systems, School of Mathematics and Physics, The University of Queensland, QLD 4072, Australia.

[3]School of Biological and Chemical Sciences, Queen Mary University of London, Mile End Road, London E1 4NS, United Kingdom

[4]Centre for Plastic Electronics, Department of Chemistry, Imperial College London, Exhibition Road, London SW7 2AZ, United Kingdom

[5]KSC, King Abdullah University of Science and Technology, Thuwal 23955-6900, Saudi Arabia

[6]Centre for Engineered Quantum Systems, Australian Institute for Nanoscale Science and Technology, and School of Chemistry, The University of Sydney, NSW 2006, Australia

[7]SPECIFIC IKC, College of Engineering, Swansea University, SA12 7AX, U.K.

Email: neher@uni-potsdam.de, j.durrant@imperial.ac.uk

1. **Polymer and fullerene structures and UV-vis absorption of the blends**
2. **WAXD crystallite size analysis**
3. **Free energy simulations**
4. **Optical spectroscopy in thin films**
5. **External quantum efficiency (EQE) of PBTTT:fullerene devices and *J-V* curves parameters**
6. **Time-delayed collection field transients (TDCF)**
7. **References**

1. Polymer and fullerene structures and UV-vis absorption of the blends

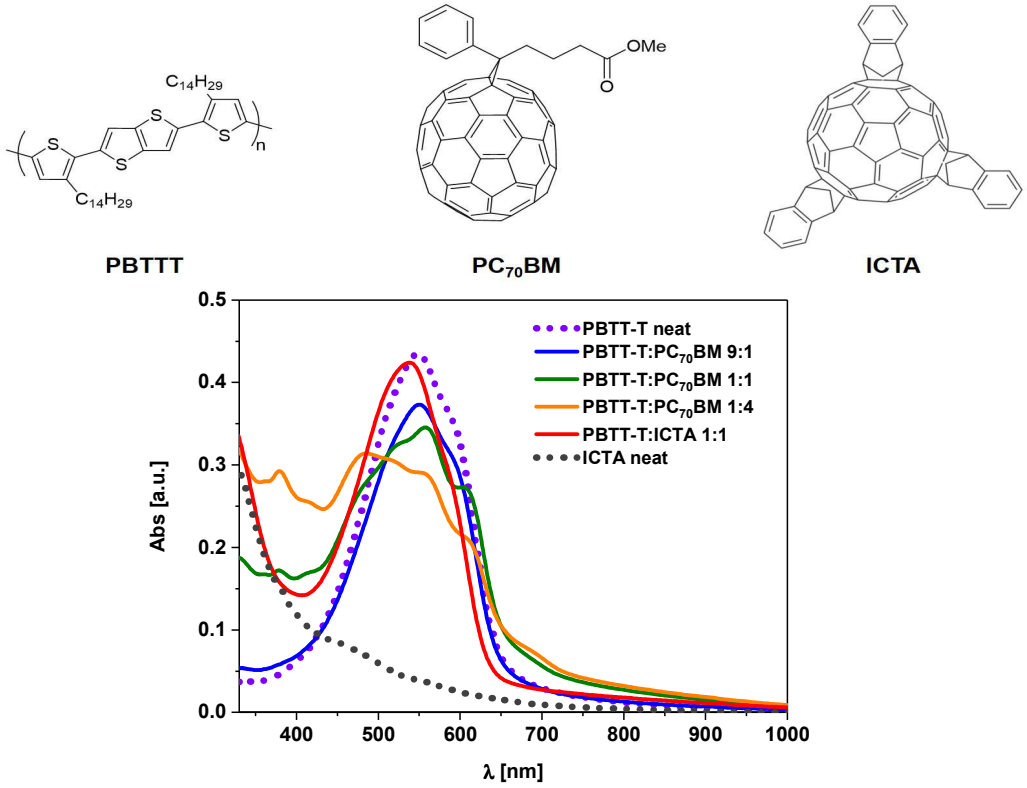

Figure S1. Chemical structures of the polymer donor and acceptors and UV-vis spectra of the corresponding neat and blend films used in this study.

2. WAXD crystallite size analysis

Scherrer equation was used to estimate the size of the crystallites for all the blends. The model assumes a spherical shape with cubic symmetry (and thus a Scherrer constant $K = 0.94$) As such, the crystallite sizes are approximate and do not take into consideration other interactions like the $\pi - \pi$ stacking in the material, which could elongate the crystallite. In order to obtain the FWHM, and the mid-point 2θ values, the first and second order diffraction peaks were fitted to a Pearson VII function, an exponential mixing of Gaussian and Lorentzian components. Table S1 shows the peak center, x_c and the FWHM as obtained from the fits, as well as the average crystallite size $\bar{L}$. It is important to remark, however that for the $PC_{70}BM$

blend films, these crystallites correspond to what has been named 'bi-molecular' or co-crystals of PBTTT with the fullerene incorporated into the side chains.[1–4]

Table S1. Fitting parameters obtained from Pearson VII fits of the WAXD lamellar peak of the blends and the respective average crystallite size obtained using Scherrer equation.

System	2θ [rad]	FWHM [rad]	L [nm]	$\bar{L}$ [nm][a]
Neat PBTTT	0.0749	0.0159	9.1	9 ± 1
	0.1503	0.0202	7.2	
9:1 PBTTT:$PC_{70}BM$	0.0735	0.0183	7.9	7.4 ± 0.3
	0.1502	0.0198	7.3	
1:1 PBTTT:$PC_{70}BM$	0.0533	0.0098	14.8	13 ± 2
	0.1010	0.0146	9.9	
1:4 PBTTT:$PC_{70}BM$	0.0526	0.0167	8.7	9 ± 1
	-	-	-	
1:1 PBTTT:ICTA	0.0759	0.0167	8.7	8 ± 1
	0.1521	0.0208	7.0	

[a] The average crystallite size $\bar{L}$, was determined by a weighted average, where the a proportional weight coefficient was given to the measurements that had less error in the fitting.

3. Free energy simulations

The simulation method used here is based on a methodology used elsewhere.[5] Individual molecules within the materials are represented as sites with a dielectric constant of $\epsilon_r = 3.5$ and are assumed to be at a temperature of $T = 300\,K$. The electron and hole are initially situated on the interface as a charge-transfer (CT) state with the hole in the PBTTT and the electron in the acceptor. The free energy of the electron-hole pair as a function of their separation *r* is then calculated with and without energetic disorder.

For the intercalated case, the phases are modelled as one-dimensional materials as shown in Figure S2, since the charges will move much faster along the chains than between them,

preventing inter-chain thermalisation. For the phase-separated system a bilayer was assumed for simplicity without being a gross simplification since charges separate within a few nanometers. The morphology was represented as two phases of three-dimensional hexagonal close-packed lattice with a planar interface between them, as shown in Figure S2.

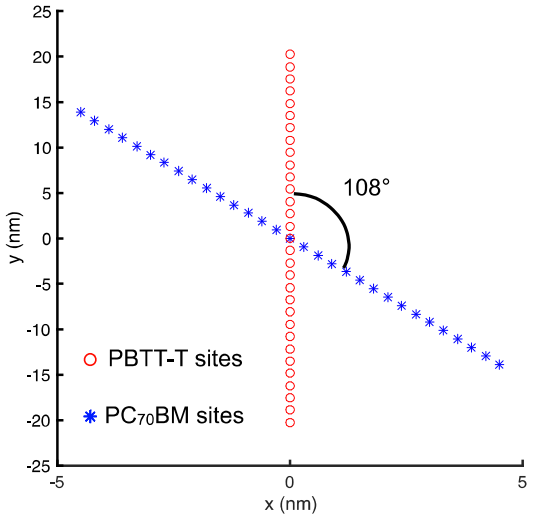

Figure S2. The model for intercalated geometry. PBTTT and $PC_{70}BM$ chains are separated by 0.5 nm (in the z direction) with an angle of 108˚ between them.[3] The inter-site spacing in PBTTT was 1.35 nm and in $PC_{70}BM$ 0.97 nm.[3]

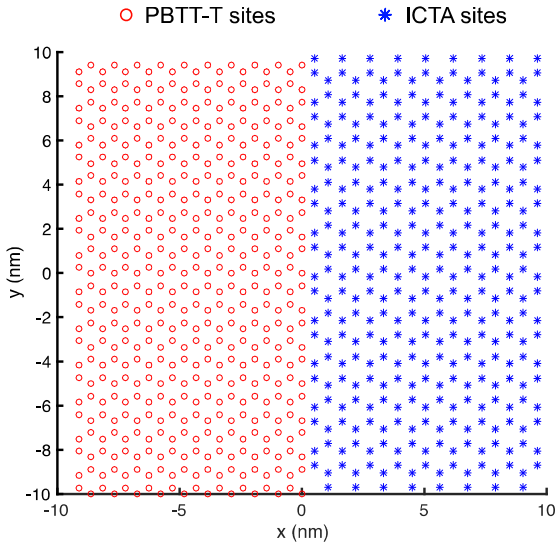

Figure S3. The model for the non-intercalated morphology. The inter-site spacing in each phase is determined from the site densities of PBTTT and ICTA, which were taken to be $1.57nm^{-3}$ and $0.79nm^{-3}$ respectively.[6,7] The nearest-neighbor distance between sites across the interface assumed to be 1 nm.

Energetically ordered case

The free energy $\Delta G(r)$ of the electron-hole pair at a separation r depends on the entropy $\Delta S(r)$. The entropy is itself determined by the number of ways to arrange the charges $\Omega(r)$, meaning that increasing r generally increases the entropy, lowering the free energy. To compare the free energy of charge separation in the two different morphologies, it is assumed that $\Omega(1\ nm) = 1$ for both cases. Without energetic disorder the site energies are the same for a given value of r, meaning that we can use the microcanonical ensemble to find the free energy of the electron-hole pair,

$$\Delta G_{ordered}(r) = U(r) - T\Delta S(r)$$

where $\Delta S(r) = k_B \ln \Omega(r)$ and $U(r)$ is the Coulomb potential between two elementary charges a distance r apart,

$$U(r) = \frac{e^2}{4\pi\epsilon_0\epsilon_r r}$$

Energetically disordered case

Organic semiconductors are disordered materials, and this disorder affects the entropy. To include energetic disorder, we draw random site energies from a normal distribution of width σ, whose typical value in organic semiconductors is $\sigma = 100$ meV. In the presence of disorder, the free energy is most easily calculated in the canonical ensemble,

$$\Delta G_{disordered}(r) = -\langle k_B T \ln Z(r) \rangle$$

where $\langle \cdots \rangle$ denotes averaging over realisations of energetic disorder. The partition function is

$$Z(r) = \sum_{\alpha=1}^{\Omega(r)} \exp\left(-\frac{U(r) + E_\alpha^e + E_\alpha^h}{k_B T}\right)$$

where the sum goes over all possible arrangements α of the electron and the hole at a distance *r* apart. Here, E_α^e and E_α^h denote the disordered energies of the electron and hole respectively for configuration α.

When the charge carriers are confined to one-dimensional channels as in the intercalated case, for a given value of *r* there are only two possible arrangements on the chains, $\Omega(r) = 2$. This means that neither entropy nor disorder have a significant effect on the free-energy of dissociation. As a result, there is no barrier to speak of - the free energy increases monotonically, meaning that it is always favourable for the charges to recombine geminately.

As discussed in ref.[5], for three-dimensional materials $\Omega(r)$ scales as r^3. This means that entropy and disorder have a greater effect on the free energy barrier than in the intercalated case. For a typical amount of energetic disorder, entropy and disorder remove the barrier to charge separation altogether, meaning that this morphology may result in less geminate recombination of the CT state.

4. Optical spectroscopy in thin films

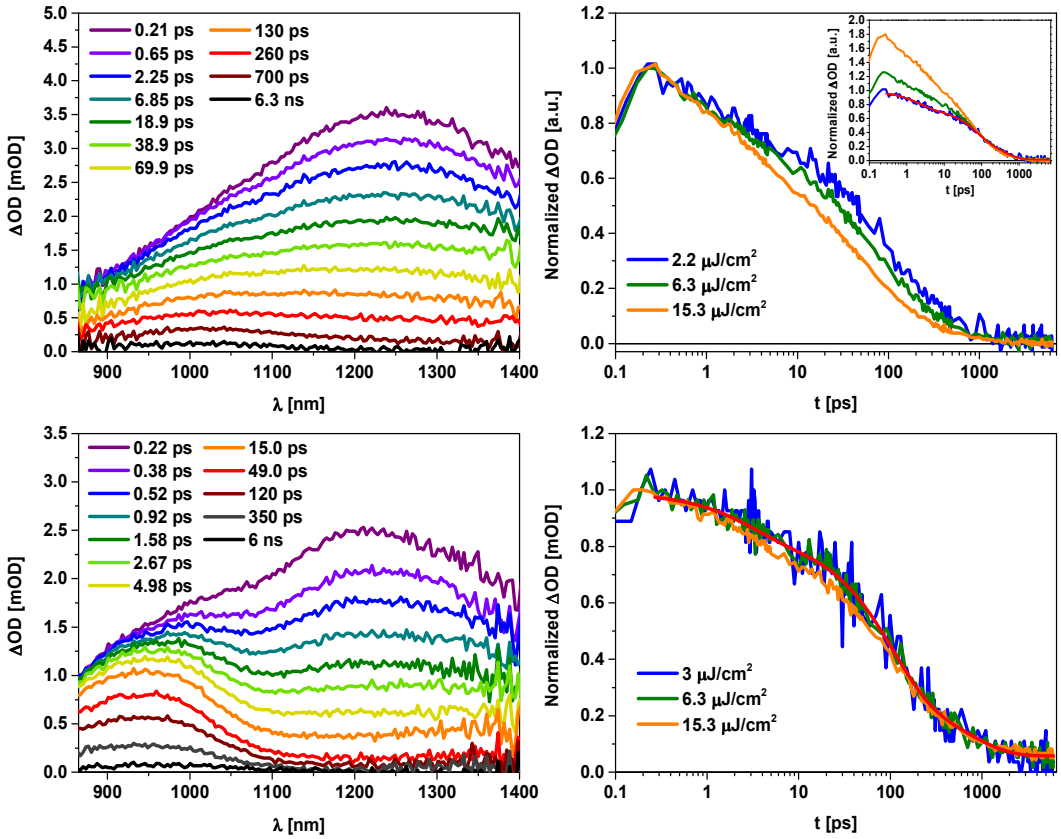

Figure S4. Transient absorption data for a representative (top) neat PBTTT thin film and (bottom) 9:1 PBTTT/$PC_{70}BM$ blend film. The left graphs show the transient absorption spectra, taken after exciting at 540 nm with 6 μJ/cm^2. The right graphs show, for the neat PBTTT the exciton photoinduced absorption kinetics taken at 1250 nm, inset is the same data, normalized at ≈ 100 ps, showing the exciton-exciton annihilation contribution. For the 9:1 PBTTT/$PC_{70}BM$ blend, kinetics of the positive polaron photoinduced absorption at 900 nm are shown. The transients have been fitted to a tri-exponential function.

Table S2. Tri-exponential fit parameters of the TAS signals shown in Figure S4 (right panels)

Fit parameters	Neat PBTTT	9:1 PBTTT:$PC_{70}BM$
A_0 [a.u.]	0.014±0.004	0.059±0.005
A_1 [a.u.]	0.25±0.01	0.16±0.01
τ_1 [ps]	2.0±0.3	2.8±0.5
A_2 [a.u.]	0.43±0.04	0.57±0.03
τ_2 [ps]	67±9	100±9
A_3 [a.u.]	0.30±0.05	0.21±0.03
τ_3 [ps]	390±60	700±200
$\bar{\tau}$ [ps]	146±20	204±50

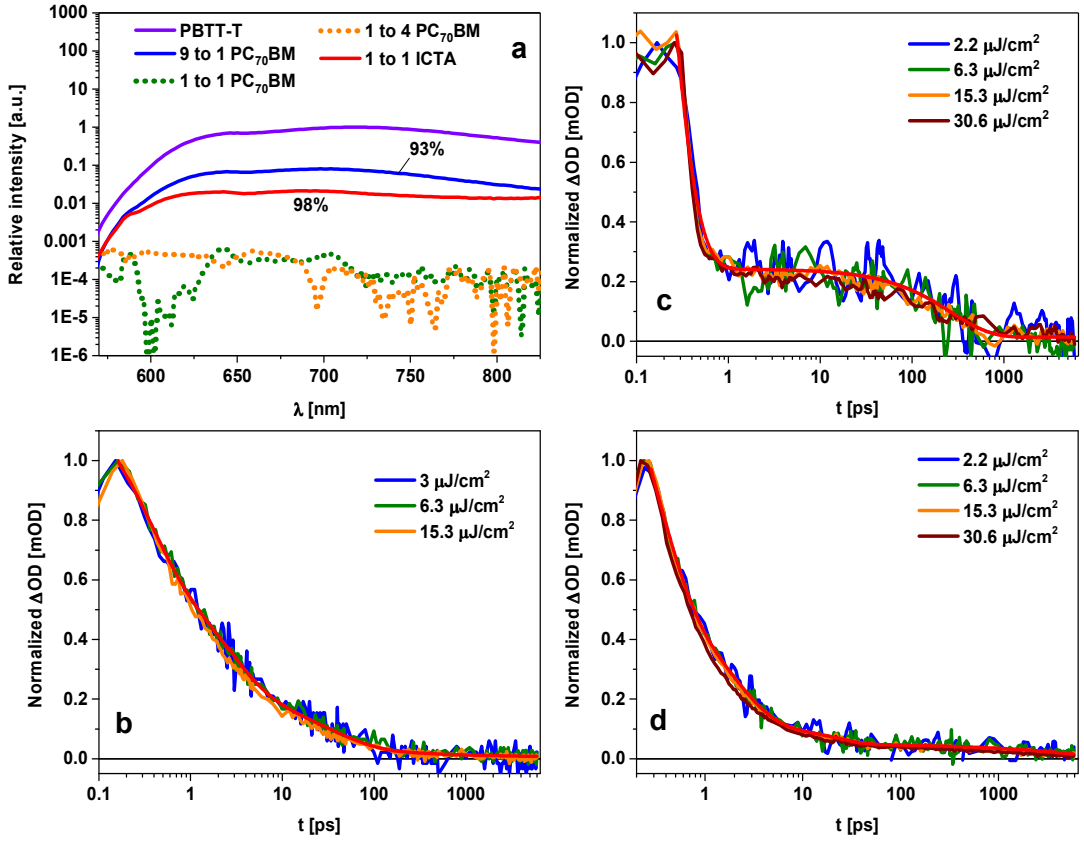

Figure S5. a) Steady-state photoluminescence (PL) emission spectra for the different blends films. Exciton photoinduced absorption kinetics after excitation at 540 nm and probed at 1250 nm for b) 9:1 PBTTT:$PC_{70}BM$ blend film, c) 1:1 PBTTT/$PC_{70}BM$ and d) 1:1 PBTTT/ICTA.

Table S3. Tri-exponential fit parameters of the TAS signals shown in Figure S5b, S5c and S5d

Fit parameters	1:1 PBTTT:$PC_{70}BM$	9:1 PBTTT:$PC_{70}BM$	1:1 PBTTT:ICTA
A_0 [a.u.]	0.003±0.001	0.009±0.002	0.017±0.001
A_1 [a.u.]	0.95±0.14	0.48±0.03	0.68±0.05
			(0.73±0.05)*
τ_1 [ps]	0.15±0.01	0.32±0.04	0.28±0.03
A_2 [a.u.]	0.05±0.002	0.35±0.02	0.25±0.02
			(0.27±0.02)*
τ_2 [ps]	266±22	2.6±0.2	1.9±0.2
A_3 [a.u.]	-	0.16±0.01	0.05±0.01
τ_3 [ps]	-	43±4	27±5
$\bar{\tau}$ [ps]	-	7.9±0.8	2.0±0.4

* Data in parenthesis indicates the percentage contribution of the decays if only two exponentials are used

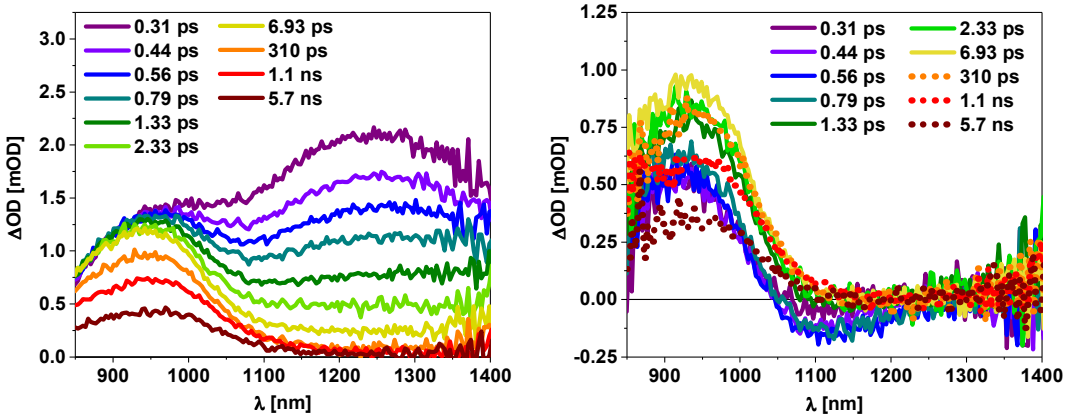

Figure S6. Transient absorption data for a representative of PBTTT:ICTA 1:1 excited at 540 with a fluence of 6 μJ/cm^2. (left) raw data and (right) data corrected by exciton absorption at 1250 nm, which kinetics are shown in Figure 4h in the manuscript.

Table S4. Multi-exponential fit parameters of the TAS signals shown in Figures 4b and 4h

Fit parameters	1:1 PBTTT:$PC_{70}BM$[a]	1:1 PBTTT:ICTA[b]
A_0 [a.u.]	0.28 ± 0.04	1.347 ± 0.007
A_1 [a.u.]	-2.1 ± 0.9	-1.71 ± 0.12 (-0.86 ± 0.06)*
τ_1 [ps]	≤ 0.15	0.33 ± 0.03
A_2 [a.u.]	1.64 ± 0.12 (0.9 ± 0.1)*	-0.29 ± 0.05 (-0.14 ± 0.03)*
τ_2 [ps]	220 ± 21	2.9 ± 0.5
A_3 [a.u.]	0.2 ± 0.1 (0.1 ± 0.05)*	0.13 ± 0.01 (0.19 ± 0.01)*
τ_3 [ps]	1800 ± 2100	160 ± 35
A_4 [a.u.]	-	0.54 ± 0.01 (0.81 ± 0.01)*
τ_4 [ps]	-	1730 ± 98

[a] τ_1 corresponds to the rise of the polaron signal. In this case only τ_2 corresponds to the geminate recombination of polarons. This is due to the long lifetime τ_3 'contamination' by an intensity-dependent phase, which could correspond to the onset of non-geminate recombination.
[b] The time constants that correspond to the rise of the polaron signal are τ_1 and τ_2 whereas τ_3 and τ_4 correspond to the geminate recombination of the polarons. Therefore the average rise signal assigned to the polaron generation is τ_{gen} = 0.7±0.1 ps, whereas the average polaron decay via recombination is τ_{recomb}= 1.43 ± 0.08 ns. Data in parenthesis indicates the percentage contribution of the decays if only two exponentials are used in each case.

Charge generation in the 1:1 PBTTT:ICTA blend

The apparent discrepancy between the 2.0 ± 0.4 ps exciton decay (Table S3) and the 0.7 ± 0.1 ps polaron generation (Table S4) comes from a 5% contribution of a long lifetime (27 ± 5 ps) of the polymer exciton in the PBTTT:ICTA blend (see Table S3). This long lifetime takes the average exciton decay from 0.72 ± 0.07 ps (τ_1 and τ_2 only) to 2.0 ± 0.4 ps (average of τ_1, τ_2 and τ_3). This small contribution does not seem to be present in the polaron rise, however we remark that to obtain Figure 4h, we corrected the data for exciton contrubution using the neat blend, which could incur into errors especially given that a large exciton delocalization is present in these blends.

5. External quantum efficiency (EQE) of PBTTT:fullerene devices and *J-V* curves parameters

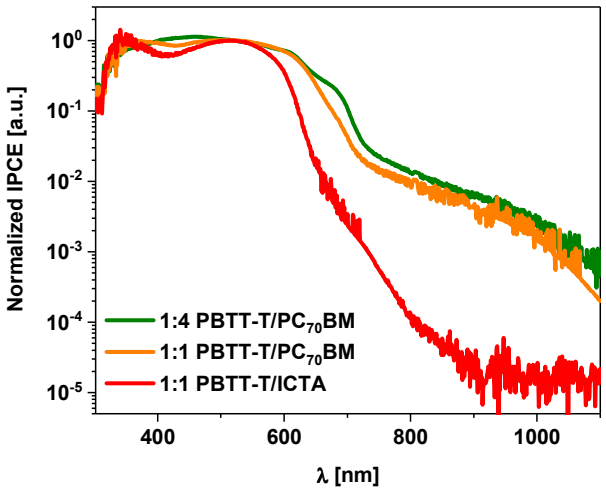

Figure S7. Steady-state EQE spectra normalized at 522 nm for the three systems herein studied, showing bound-charge absorption in the 1:1 and 1:4 PBTTT/$PC_{70}BM$ devices.

Table S5. Efficiency figures for the devices used in TDCF

	ICTA	$PC_{70}BM$	
	1:1	**1:1**	**1:4**
J_{SC} **(mAcm^{-2})**	0.43	2.37	4.76
V_{OC} **(V)**	0.64	0.53	0.52
FF	0.27	0.35	0.42
PCE (%)	0.07	0.43	1.02

6. Time-delayed collection field transients (TDCF)

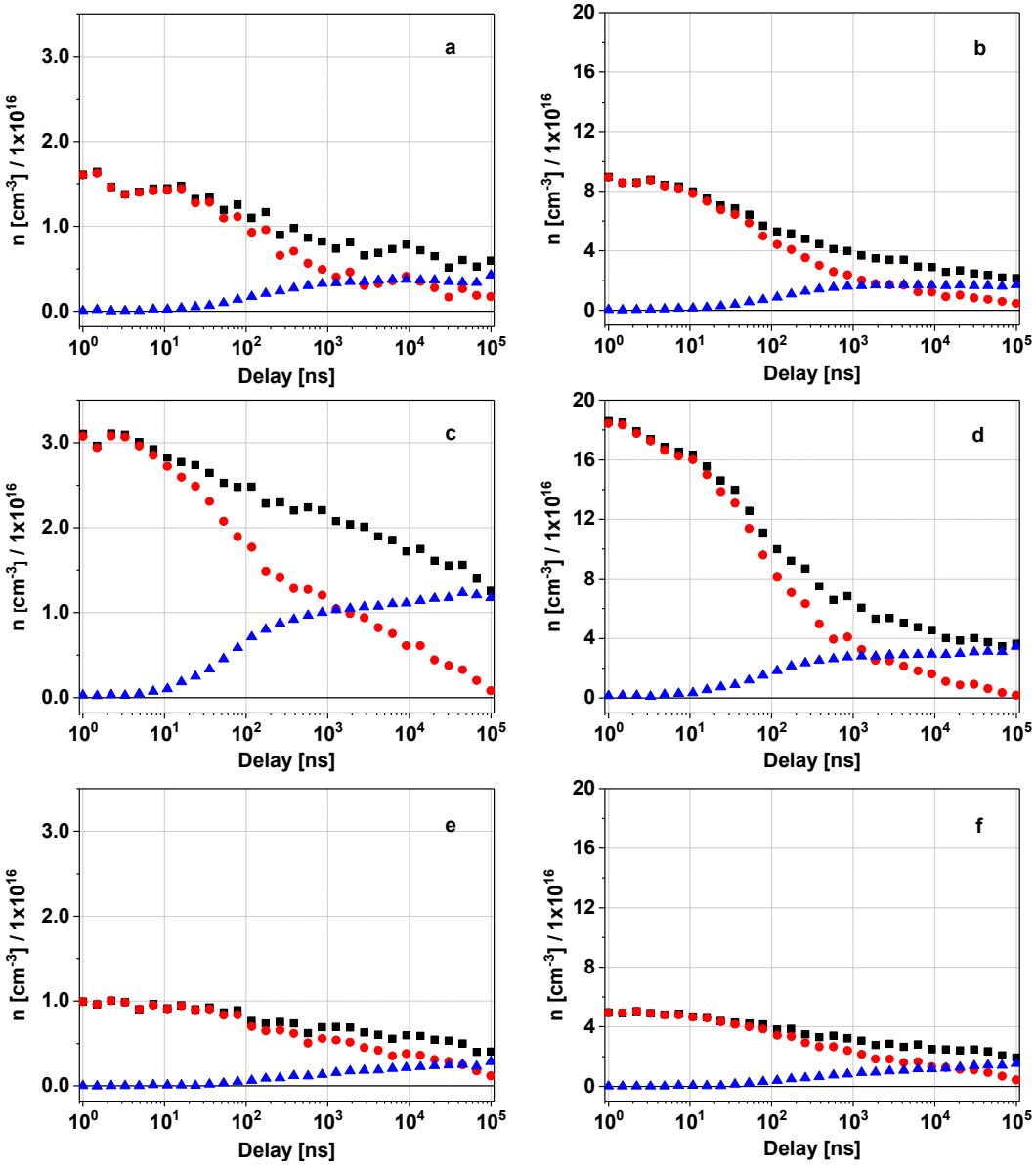

Figure S8. Absolute charge density transients obtained from TDCF at 0.4 V prebias, left at ≈ 0.6 μJ/cm^2 and right at ≈ 6.8 μJ/cm^2. In black, the total charge density, n_{tot} used in Figures 4 and 5. In red, the collection charge density n_{coll}, and in blue the extraction charge density n_{pre} for representative a), b) 1:1 PBTTT/PC$_{70}$BM devices; c), d) 1:4 PBTTT/PC$_{70}$BM devices and e), f) 1:1 PBTTT/ICTA devices.

References

(1) Miller, N. C.; Sweetnam, S.; Hoke, E. T.; Gysel, R.; Miller, C. E.; Bartelt, J. A.; Xie, X.; Toney, M. F.; McGehee, M. D. Molecular Packing and Solar Cell Performance in Blends of Polymers with a Bisadduct Fullerene. *Nano Lett.* **2012**, *12*, 1566–1570.

(2) Miller, N. C.; Cho, E.; Gysel, R.; Risko, C.; Coropceanu, V.; Miller, C. E.; Sweetnam, S.; Sellinger, A.; Heeney, M.; McCulloch, I. et al. Factors Governing Intercalation of Fullerenes and Other Small Molecules between the Side Chains of Semiconducting Polymers Used in Solar Cells. *Adv. Energy Mater.* **2012**, *2*, 1208–1217.

(3) Miller, N. C.; Cho, E.; Junk, M. J. N.; Gysel, R.; Risko, C.; Kim, D.; Sweetnam, S.; Miller, C. E.; Richter, L. J.; Kline, R. J.; et al. Use of X-Ray Diffraction, Molecular Simulations, and Spectroscopy to Determine the Molecular Packing in a Polymer-Fullerene Bimolecular Crystal. *Adv. Mater.* **2012**, *24*, 6071–6079.

(4) Buchaca-Domingo, E.; Ferguson, a. J.; Jamieson, F. C.; McCarthy-Ward, T.; Shoaee, S.; Tumbleston, J. R.; Reid, O. G.; Yu, L.; Madec, M.-B.; Pfannmöller, M., et al. Additive-Assisted Supramolecular Manipulation of Polymer:fullerene Blend Phase Morphologies and Its Influence on Photophysical Processes. *Mater. Horizons* **2014**, *1*, 270.

(5) Hood, S. N.; Kassal, I. Entropy and Disorder Enable Charge Separation in Organic Solar Cells. *J. Phys. Chem. C* **2016**, *7*, 4495–4500.

(6) Poelking, C.; Cho, E.; Malafeev, A.; Ivanov, V.; Kremer, K.; Risko, C.; Brédas, J. L.; Andrienko, D. Characterization of Charge-Carrier Transport in Semicrystalline Polymers: Electronic Couplings, Site Energies, and Charge-Carrier Dynamics in Poly(bithiophene-Alt-Thienothiophene) [PBTTT]. *J. Phys. Chem. C* **2013**, *117* (4), 1633–1640.

(7) Napoles-Duarte, J. M.; Reyes-Reyes, M.; Ricardo-Chavez, J. L.; Garibay Alonso, R.; Lopez-Sandoval, R. Effect of Packing on the Cohesive and Electronic Properties of Methanofullerene Crystals. *Phys. Rev. B.* **2008**, *78*, 1–7.